Modelling natural and mixed convection in obstructed channels

Marcela Cruchaga and Diego Celentano
Departamento de Ingeniería Mecánica, Universidad de Santiago de Chile, Santiago de Chile, Chile

Received October 2001
Revised July 2002
Accepted August 2002

Keywords *Convection, Finite element analysis*

Abstract *The modelling of steady-state natural and mixed convection in obstructed channels is presented. The two-dimensional numerical analysis is carried out with a finite element thermally coupled incompressible flow formulation written in terms of the primitive variables of the problem and solved via a generalized streamline operator technique. Natural convection is studied in several vertical channel configurations for a wide range of Rayleigh numbers while mixed convection is analysed in a horizontal channel with a built-in rectangular cylinder for different Reynolds and Grashof numbers. The results obtained in this work are validated with available experiments and other existing numerical solutions.*

Nomenclature

a = vertical channel width
$\mathbf{b}$ = body force vector, $\mathbf{g}[1 - \propto(T - T_{\text{ref}})]$
c = specific heat
C_{d} = drag coefficient
C_{l} = lift coefficient
C_x = friction coefficient, $2\,\partial U/\partial y$
g = gravity value
$\mathbf{g}$ = gravity vector
Gr = Grashof number, Ra/Pr
h = thickness of the obstruction
H = horizontal channel height
k = conductivity coefficient
L = vertical channel height
L_1 = height of the obstruction on the left wall from the vertical channel entrance
L_2 = height of the obstruction on the right wall from the vertical channel entrance
$\mathbf{n}$ = outward unit normal vector to Γ
Nu = average Nusselt number, $1/L \int_L \text{Nu}_y \, \text{d}y$
Nu_x = local Nusselt number for the horizontal channel, $(T_{\text{w}} - T_{\text{in}})/(T_{\text{w}} - T_{\text{b}})\,\partial T/\partial y$
Nu_y = local Nusselt number for the vertical channel, $\text{a}\nabla T \cdot \mathbf{n}$
p = pressure
Pr = Prandtl number, μc/k
r = radius of the obstruction
Ra = Rayleigh number, $g\alpha(T_{\text{w}} - T_{\text{in}})a^3 c\rho^2/k\mu$
Re = Reynolds number, $U_{\text{av}} H\rho/\mu$
T = temperature
T_{b} = bulk temperature, $1/H \int_{\text{H}} T\text{d}y$ for $0 < x < 2H$; $2.25H < x < 6H$ $1/(0.375H) \int_{0.375H} T\text{d}y$ for $2H \leq x \leq 2.25H$ and $0 \leq y \leq 0.375H$; $0.75H \leq y \leq H$
U = horizontal component of the velocity
U_{av} = average velocity at the inflow
$\mathbf{v}$ = velocity vector
V = vertical component of the velocity
w = width of the obstruction
x = horizontal spatial coordinate
y = vertical spatial coordinate
Y = time interval of interest

The support provided by the Chilean Council for Research and Technology CONICYT (FONDECYT Project No. 1020029) and the Department of Scientific and Technological Research at the University of Santiago de Chile DICYT-USACH is gratefully acknowledged.

International Journal of Numerical Methods for Heat & Fluid Flow
Vol. 13 No. 1, 2003
pp. 57-85

0961-5539
DOI 10.1108/09615530310456769

$\mathbf{R}_V$ = flow residual vector
$\mathbf{F}_V$ = force vector
$\mathbf{M}$ = mass matrix
$\mathbf{K}_V$ = advection-diffusion matrix
$\mathbf{V}$ = flow nodal unknowns vector (velocity and pressure)
$\mathbf{R}_T$ = thermal residual vector
$\mathbf{F}_T$ = external heat flux vector
$\mathbf{C}$ = capacity matrix
$\mathbf{K}$ = conductivity matrix
$\mathbf{K}_{ad}$ = thermal advection matrix
$\mathbf{T}$ = nodal temperature vector
α = volumetric thermal dilatation coefficient
ε = rate of deformation tensor, $1/2\,(\nabla \times \mathbf{v} + \mathbf{v} \times \nabla)$
ρ = density
μ = dynamic viscosity
∇ = spatial gradient operator
Γ = smooth boundary
Ω = arbitrary open bounded domain

Subscripts

in = inlet
ref = reference value
w = channel wall

Superscripts

$\cdot$ = time derivative

1. Introduction

The study of natural convection becomes relevant in many engineering problems where the flow and heat transfer conditions are strongly affected by buoyancy forces. Moreover, a wide range of practical applications also involve the analysis of mixed convection flows. In particular, the understanding of such phenomena is important in the design of electronic equipment, heat exchangers, reactors and energy storage systems. Due to this, several experimental and numerical studies have been carried out by different researchers in order to evaluate the thermal behaviour and the flow pattern of convection induced flows in geometrical configurations which commonly appear in engineering designs: heat conducting planar channels (Aung and Worku, 1986; Burch *et al.*, 1985; Maughan and Incropera, 1987), natural convection in thermosyphons (Islam *et al.*, 1998; Mohamad and Sezai, 1997), flow and heat transfer analysis in backward-facing steps (Baek *et al.*, 1993; Cruchaga, 1998; Hong *et al.*, 1993; Iwai *et al.*, 2000a, b; Tsui and Wang, 1995), assessment of the effects of obstructions on the thermo-fluid behaviour in ducts (Bejan *et al.*, 1995; Elenbass, 1942; Naylor and Tarasuk, 1993a, b; Said and Krane, 1990; Viswatmula and Amin, 1995) and non-isothermal flow past heated bodies in horizontal channels (Cesini *et al.*, 1999; Chang *et al.*, 1988; Kaminski *et al.*, 1995; Karniadakis, 1988; Leung *et al.*, 2000; Ramaswamy and Jue, 1992; Sadeghipour and Hannani, 1992; Shuja *et al.*, 2000; Wang and Liu, 1992). The modelling of such applications has been approached by using numerical solution algorithms defined in the frameworks of finite difference (Aung and Worku, 1986; Burch *et al.*, 1985; Chang *et al.*, 1988; Iwai *et al.*, 2000a, b), finite volume (Baek *et al.*, 1993; Hong *et al.*, 1993; Leung *et al.*, 2000; Mohamad and Sezai, 1997; Shuja *et al.*, 2000; Tsui and Wang, 1995; Wang and Liu, 1992), finite element (Bejan *et al.*, 1995; Cesini *et al.*, 1999; Cruchaga, 1998; Kaminski *et al.*, 1995; Naylor and Tarasuk, 1993a; Ramaswamy and Jue, 1992; Sadeghipour and Hannani, 1992; Said and Krane, 1990; Viswatmula and Amin, 1995)

and spectral (Karniadakis, 1988) methods. In addition, some of these numerical predictions have been validated with experiments (Baek *et al.*, 1993; Elenbass, 1942; Islam *et al.*, 1998; Kaminski *et al.*, 1995; Maughan and Incropera, 1987; Naylor and Tarasuk, 1993b; Said and Krane, 1990; Wang and Liu, 1992).

This work presents a numerical analysis of natural and mixed convection in obstructed channels applying an alternative finite element thermally coupled incompressible flow formulation based on a generalized streamline operator technique and written in terms of the primitive variables of the problem: velocity, pressure and temperature (Celentano *et al.*, 2001; Cruchaga and Celentano, 2000). The main features of this formulation are related to the convective and pressure numerical stabilization contributions and the least squares form of the incompressibility constraint both intrinsically encompassed by this methodology which provides, among others, the possibility to adopt equal order interpolation functions for the primitive variables and precludes the use of penalty procedures. This numerical approach is particularly well suited for modelling problems at moderate-to-high Rayleigh numbers (Ra) and Reynolds numbers (Re). The governing equations and the corresponding weak form used to obtain this discretized formulation are briefly described in Section 2.

The objective of this work is the experimental and numerical validation of the above-mentioned formulation in the analysis of the flow and thermal responses of air in two-dimensional obstructed channels. An additional goal is the extension of the study to higher Ra and Re with respect to those previously reported in the literature. To this end, natural convection is studied in vertical ducts for several Ra ranging from 10^2 to 10^6 in channels with circular and multiple rectangular wall blocks obstructions. In particular, different locations of the obstructions and channel aspect ratios (Ar) are evaluated for the latter case. Moreover, smooth channel solutions are also obtained for comparison purposes. The second problem consists of the analysis of mixed convection in a horizontal channel with a built-in rectangular cylinder for different Re (100 and 500) and Grashof numbers (Gr; from 0 to 320,000). The buoyancy forces are assumed to be governed by the Boussinesq approximation since no significant air density changes are expected for the temperature ranges involved in both applications. The steady-state results obtained in this work include temperature, streamline and pressure spatial contours, local Nusselt number (Nu) and friction coefficient distributions along the channel walls, average Nu and, finally, drag and lift coefficients. The numerical predictions for both problems are discussed and validated with available experiments and other existing numerical solutions in Section 3.

2. Governing equations and finite element formulation

The basic formulation for incompressible laminar flow problems considering a Newtonian fluid can be described by the momentum, continuity and energy equations written as (Malvern, 1969):

$$\rho\dot{\mathbf{v}} + \rho(\mathbf{v}\cdot\nabla)\mathbf{v} + \nabla p - \nabla\cdot(2\mu\varepsilon) = \rho\mathbf{b} \quad \text{in } \Omega\times \mathrm{Y} \tag{1}$$

$$\nabla\cdot\mathbf{v} = 0 \quad \text{in } \Omega\times \mathrm{Y} \tag{2}$$

$$\rho c(\dot{T} + \mathbf{v}\cdot\nabla T) = \nabla(k\nabla T) \quad \text{in } \Omega\times \mathrm{Y} \tag{3}$$

together with adequate initial and boundary conditions. As usual, the buoyancy effects are included in the specific body force vector written according to the Boussinesq approximation. In these equations, isotropic heat conduction is assumed, no specific heat source is considered and the energy term derived from mechanical viscous effects is neglected.

The weak formulation of the differential equations system (1-3) is obtained in the context of the finite element method (Huang and Usmani, 1994; Zienkiewicz and Taylor, 1989) by using a generalized streamline operator technique initially developed for isothermal flows (Cruchaga and Oñate, 1997, 1999) and subsequently extended to non-isothermal situations (Celentano *et al.*, 2001; Cruchaga and Celentano, 2000). Aimed at avoiding numerical oscillations normally present in dominant convective problems, this incompressible thermally coupled flow formulation accounts for stabilization contributions similar to those provided by other approaches, i.e. stabilization of the convective terms [the well-known streamline-upwind/Petrov-Galerkin (SUPG) method (Brooks and Hughes, 1982)], pressure stabilization terms to tackle the incompressibility constraint [the Galerkin least squares (GLS) approach (Hughes and Mallet, 1986) and the pressure-stabilizing/Petrov-Galerkin (PSPG) formulation (Tezduyar *et al.*, 1992)] and the least squares form of the continuity equation (Behr *et al.*, 1993). This methodology enables the use of equal order spatial interpolation functions for the primitive variables of the problem (velocity, pressure and temperature), may handle with meshes composed of regular and/or distorted elements and, moreover, does not require penalization techniques as well as tuning parameters defined outside the model. The derived residual vectors for the spatially discretized equations can be written in a compact manner as (Celentano *et al.*, 2001; Cruchaga and Celentano, 2000):

$$\begin{aligned} \mathbf{R}_V &\equiv \mathbf{F}_V - \mathbf{M}\dot{\mathbf{V}} - \mathbf{K}_V\mathbf{V} = 0 \\ \mathbf{R}_T &\equiv \mathbf{F}_T - \mathbf{C}\dot{\mathbf{T}} - (\mathbf{K} + \mathbf{K}_{\mathrm{ad}})\mathbf{T} = 0 \end{aligned} \tag{4}$$

that, respectively, represent the flow equations $\mathbf{R}_V$ (motion and continuity) and the energy equation $\mathbf{R}_T$ both including the corresponding boundary conditions. In the flow residual, the following contributions can be identified: the Boussinesq approximation in the force vector $\mathbf{F}_V$, the diffusive and convective terms together with the incompressibility condition in the advection-diffusion

matrix $\mathbf{K}_V$ and the inertial effects in the mass matrix $\mathbf{M}$. On the other hand, the energy terms can clearly be seen in the thermal residual composed of the external heat flux vector $\mathbf{F}_T$, the capacity matrix $\mathbf{C}$, the conductivity matrix $\mathbf{K}$ and the thermal advection matrix $\mathbf{K}_{\text{ad}}$. Details of the element expressions for these matrices and vectors can be found in Cruchaga and Celentano (2000). In addition, the temporal discretization of the flow nodal unknowns and nodal temperature vectors $\mathbf{V}$ and $\mathbf{T}$ is performed using a Euler backward scheme (Huang and Usmani, 1994; Zienkiewicz and Taylor, 1989). Furthermore, the coupled system of equation (4) is solved via a staggered technique avoiding in this way some practical difficulties of the full monolithic solution, e.g. large computer memory requirements. Thus, each equation is separately solved through an incremental-iterative scheme applying a Newton-Raphson type algorithm. In order to preserve the coupling degree of the system, the coupled solution is iteratively achieved in the same time step by means of locally converged flow and thermal solutions obtained in a consecutive manner such that the global convergence is attained when local convergences are simultaneously fulfilled for both residuals. In this context, during the local iterative solution procedure, the flow equation is solved at a fixed temperature distribution while a known velocity field is considered for the energy equation computation.

Steady-state solutions obtained using this methodology are presented in the numerical examples of the next section. These numerical predictions have been mainly computed through the steady-state version of system (4) (i.e. neglecting the contributions of $\boldsymbol{M}$ and $\boldsymbol{C}$). However, for problems with large Ra (or Gr) and Re, stationary solutions have been achieved via a transient analysis described by system (4) since better convergence rates have been found for these particular cases.

3. Numerical examples

3.1 Natural convection in vertical channels

Different geometries of vertical channels previously studied by other authors (Elenbass, 1942; Said and Krane, 1990; Viswatmula and Amin, 1995) are also analysed in the present work with the aim of checking the performance of the methodology briefly described in Section 2. In particular, the analysis is focused on the validation of the obtained results with experimental and numerical data, the comparison between the flow pattern and heat transfer conditions at different obstruction configurations and the extension to situations with higher Ra. To this end, two-dimensional air natural convection flow computations at a Prandtl number (Pr) of 0.71 with the gravity acting in the vertical downward direction are performed in the channels shown in Figure 1: a smooth duct (case A), a channel with a circular obstruction at the middle of its height (case B) and channels with two rectangular wall blocks (case C). Case A is studied at different Ar ($\text{Ar} = a/L$) not only to perform an experimental validation of the numerical results but also to evaluate the effects

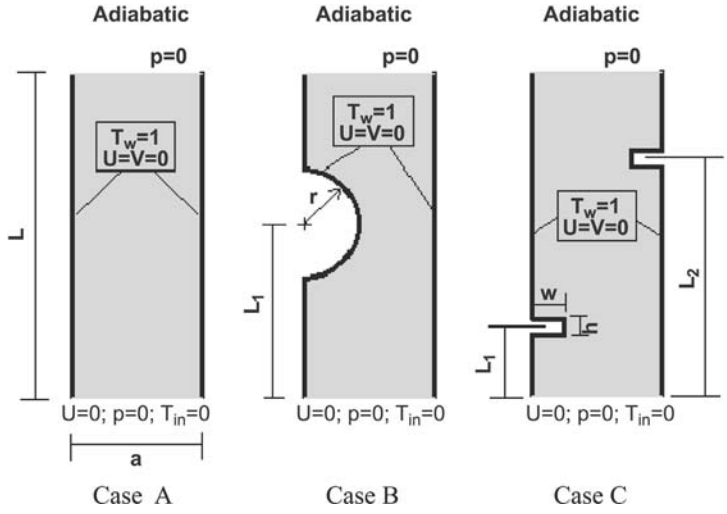

Figure 1.
Natural convection in vertical channels. Geometries and boundary conditions

of the obstructions on the thermo-fluid response when comparing this reference solution with those corresponding to cases B and C. Moreover, the proposed methodology is assessed in case B with available experimental and numerical results (Said and Krane, 1990). On the other hand, the effects of multiple obstructions located at two heights of the channel walls are studied in case C for different Ar (0.2 and 0.3) and Ra (10^2, 10^3, 10^4, 10^5 and 10^6). Numerical results for the first three Ra values have been reported in Viswatmula and Amin (1995) and, therefore, they are used to verify the current numerical predictions in these configurations. Additional geometrical parameters, Ar and Ra considered in the analysis for cases A, B and C are summarized in Table I. The associated physical vertical channel heights for different Ar and Ra considering thermophysical air properties at 20°C (i.e. $\rho = 1\,\mathrm{kg/m^3}$, $\mu = 1.8 \times 10^{-5}\,\mathrm{kg/ms}$, $c = 1,000\,\mathrm{J/kg°C}$, $k = 0.025\,\mathrm{W/m°C}$, $\alpha = 3.66 \times 10^{-3}$ and $g = 9.8\,\mathrm{m/s^2}$) and $T_w - T_{in} = 1$°C are shown in Table II.

Table I.
Natural convection in vertical channels. Characteristic lengths for different geometries and Ra analysed

		Ar = a/L	r/L	L_1/L	L_2/L	w/L	h/L	Ra
Case A (smooth channel)		0.2727	–	–	–	–	–	2×10^2, 10^3 and 2×10^4
		0.2						10^2, 10^3, 10^4, 10^5 and 10^6
		0.3						
Case B		0.2727	0.091	0.5	–	–	–	2×10^4
Case C	Geometry I	0.2	–	0.25	0.75	0.0667	0.01334	10^2, 10^3, 10^4, 10^5 and 10^6
	Geometry II	0.2		0.5	0.5			
	Geometry III	0.3		0.25	0.75			
	Geometry IV	0.3		0.5	0.5			

The boundary conditions considered in the computations are also shown in Figure 1. Non-slip boundary conditions are assumed for the velocity on the channel walls (indicated with dark solid lines in the schematic layout of Figure 1). The horizontal velocity component is fixed at zero in the inflow (bottom) section where, in addition, the pressure is also fixed at zero in order to consider a unique atmospheric relative pressure. A dimensionless unit temperature is fixed on the channel walls and a zero value is adopted at the inflow section for such variable.

The finite element meshes used in the simulations are composed of nearly 7,400 four-noded standard isoparametric elements (about 40 elements in the channel width) and 7,600 nodes. The elements are generally regular except for the distorted elements considered around the circular obstruction of case B.

The results obtained in the present work for a smooth channel (case A) with Ar = 0.2727 are presented in Figure 2 where the average Nu is plotted against

Table II.
Natural convection in vertical channels. Physical vertical channel heights L (in mm) for different Ar and Ra considering thermophysical air properties at 20°C and $T_w - T_{in} = 1$°C

Ar	Ra 10^2	2×10^2	10^3	10^4	2×10^4	10^5	10^6
0.2	53.9	–	116.1	250.2	–	539.1	1161.5
0.2727	–	49.8	85.2	–	231.2	–	–
0.3	35.9	–	77.4	116.8	–	359.1	774.3

Notes: the other physical channel sizes (a, r, L_1, L_2, w and h) can be obtained from the corresponding ratios indicated in Table I.

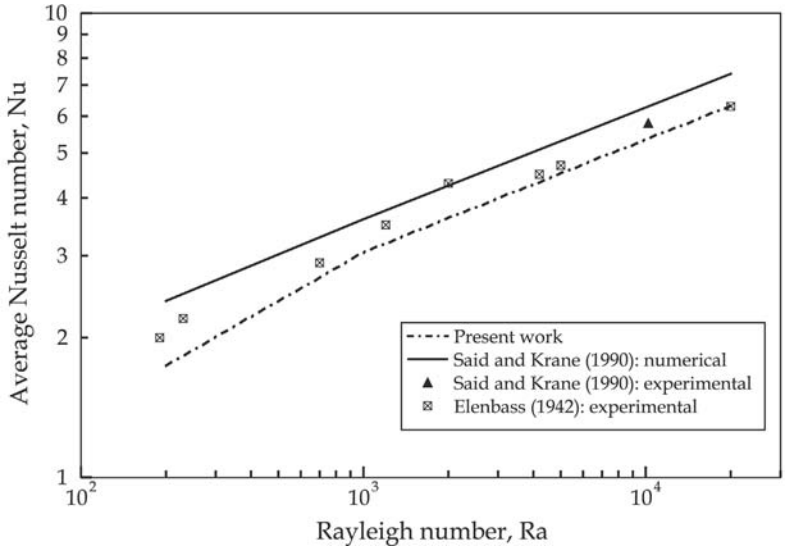

Figure 2.
Natural convection in vertical channels. Average Nu for different Ra in a smooth channel with an Ar of 0.2727

the Ra. Experimental measurements (Elenbass, 1942; Said and Krane, 1990) and existing numerical results (Said and Krane, 1990) are also included for comparison. A very good agreement between the predictions of the present analysis and the experiments can be observed. The obtained numerical values, systematically below the experimental ones, present smaller dispersions than those reported in Said and Krane (1990).

A study of smooth channels with Ar of 0.2 and 0.3 is performed in order to check the numerical behaviour in the analysed range of Ra and, in addition, to compute a reference solution for further comparison of the thermo-fluid response with those obtained for obstructed channels. The local Nu along the vertical walls is plotted in Figure 3. For a given Ar, the local Nu increases with the Ra due to the development of larger gradients close to the walls. When the Ar increases, slightly larger local Nu are obtained as a consequence of greater variations in the temperature field. Both effects can be also appreciated in the average Nu versus Ra curves depicted in Figure 4. The differences between the average Nu curves for $Ar = 0.2$ and 0.3 decrease at higher Ra remaining almost constant for $Ra \geq 10^3$ approximately. The isotherm contours for the studied Ar and Ra are presented in Figure 5 (plotted 0.1 apart) confirming once again the trends already discussed.

Numerical and experimental local Nu distributions along the obstructed and unobstructed walls for the channel with a circular obstruction are shown in Figure 6 for $Ar = 0.2727$ and $Ra = 2 \times 10^4$ (case B). Although a little overall influence of the obstacle on the Nu distribution along the unobstructed wall is observed since this curve does not present large variations in comparison with that of the smooth channel (see Figure 3), a noticeable increment can be appreciated in front of the obstruction. The local Nu distribution along the obstructed wall shows lowest values at the two intersections between the obstruction and the wall. As the velocity of the flow increases in the vicinity of the obstacle, Nu also increases up to a local maximum value. As can be seen, the numerical profiles satisfactorily match the experimental values. A slight discrepancy in the numerical results can be observed close to the bottom corner attributable to the singularity caused by the temperature boundary conditions imposed on the wall and air at the inflow section. This fact is also reflected in the high local Nu computed at such position for all the cases studied. Moreover, the isotherms, streamlines and pressure contours obtained in the present analysis are plotted in Figure 7. A thermal boundary layer is formed on each plate with larger gradients at the upstream obstacle wall. This trend agrees with the physical observations through interferograms reported in Said and Krane (1990). Owing to the reduction of the channel cross section at the obstructed zone, the density of streamlines increases, in accordance with the vertical velocity, enhancing the heat transfer conditions in that region (see Figure 6). The vertical velocity component and temperature distributions at different horizontal sections of the channel can be found in Figure 8 where a comparison with

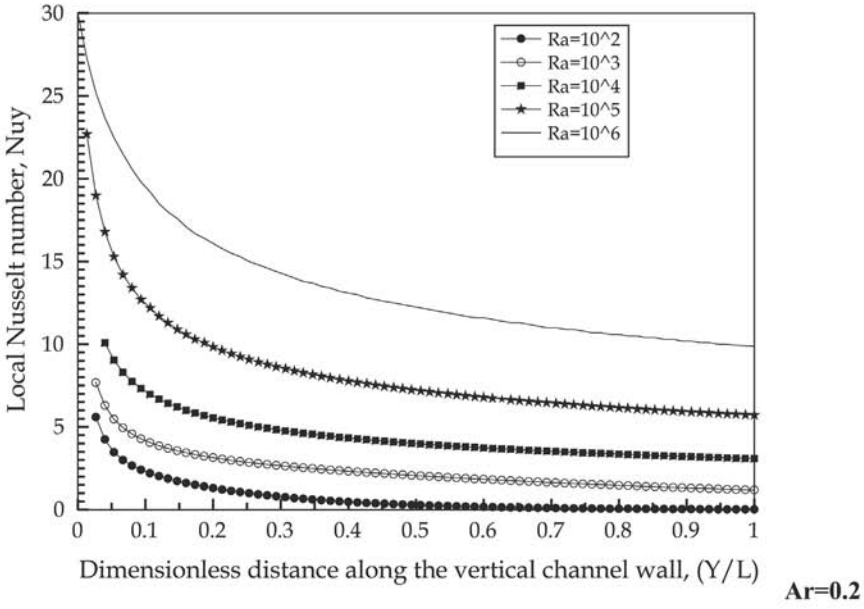

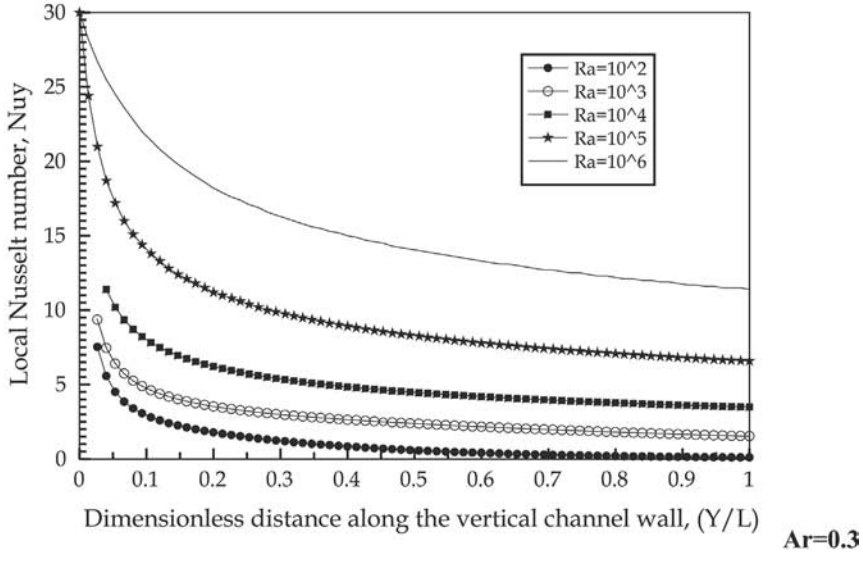

Figure 3.
Natural convection in vertical channels. Local Nu distributions in a smooth channel for different Ar and Ra

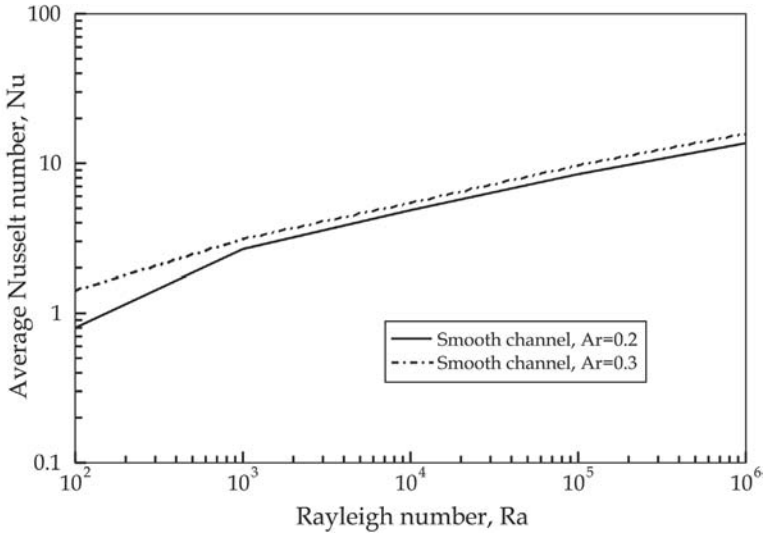

Figure 4.
Natural convection in vertical channels. Average Nu in a smooth channel with different Ar and Ra

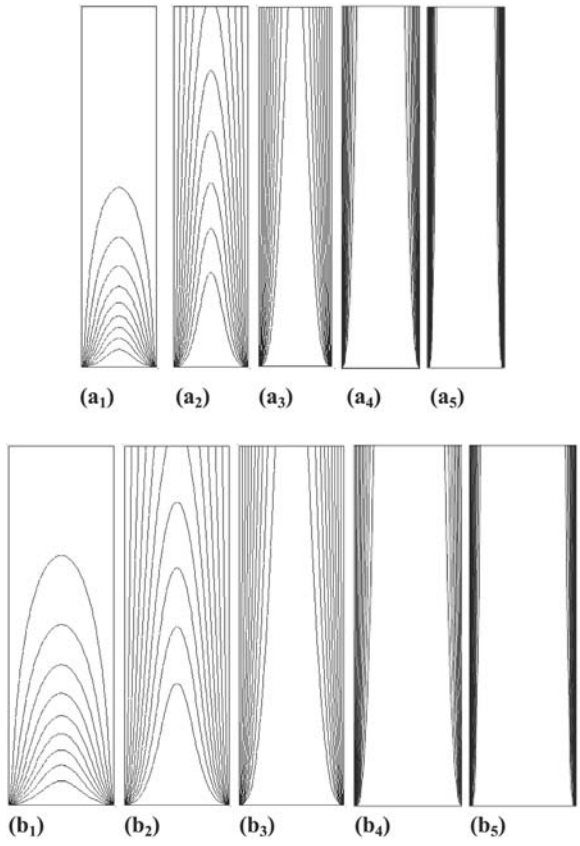

Figure 5.
Natural convection in vertical channels. Isotherms (plotted 0.1 apart) in a smooth channel for different Ar and Ra. Ar 0.2: (a_1) Ra=10^2, (a_2) Ra=10^3, (a_3) Ra=10^4, (a_4) Ra=10^5, (a_5) Ra=10^6. Ar 0.3: (b_1) Ra=10^2, (b_2) Ra=10^3, (b_3) Ra=10^4, (b_4) Ra=10^5, (b_5) Ra=10^6

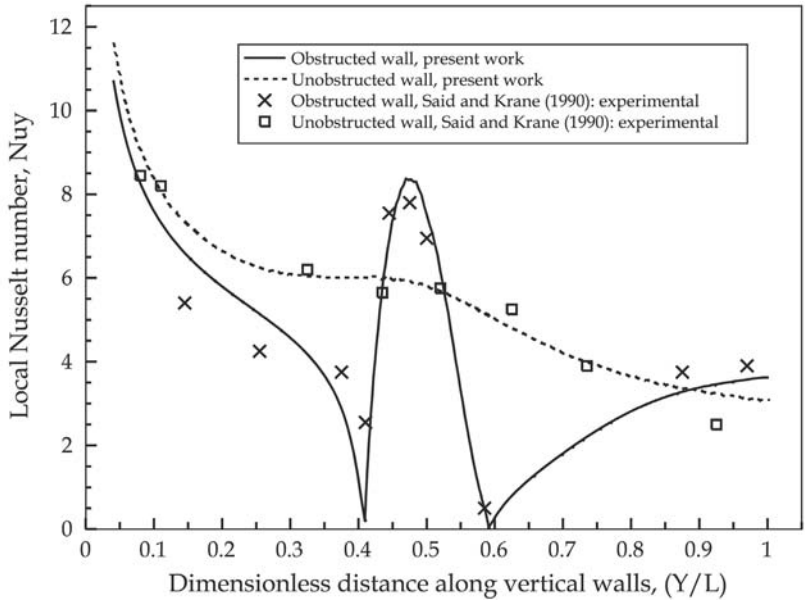

Figure 6.
Natural convection in vertical channels. Local Nu distributions in a channel with a circular obstruction at the middle of its height with an Ar of 0.2727 for $Ra = 2 \times 10^4$

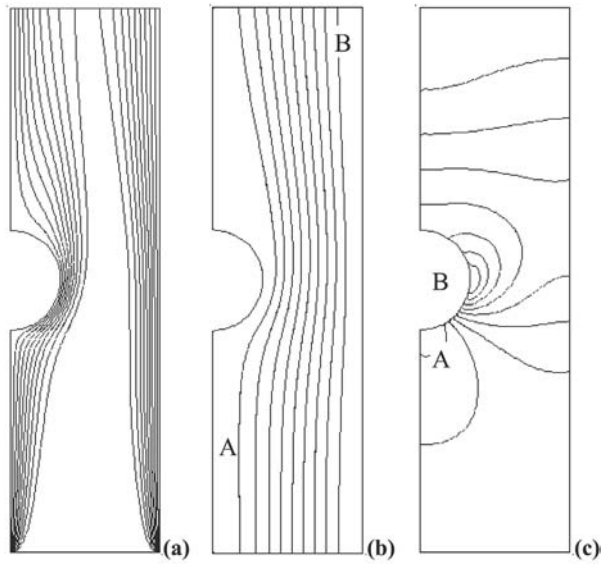

Figure 7.
Natural convection in vertical channels. Channel with a circular obstruction at the middle of its height with an Ar of 0.2727 for $Ra = 2 \times 10^4$: (a) isotherms (plotted 0.1 apart), (b) streamlines ($\varphi_A = -0.95$, $\varphi_B = -9.21$, plotted $\Delta\varphi = 1.03$ apart), and (c) pressure contours ($p_A = 0.083$, $p_B = -0.470$, plotted $\Delta p = 0.069$ apart)

the numerical results reported in Said and Krane (1990) are also included. The vertical velocity profile appears to be parabolic at the inflow and outflow sections while a sharp distribution is found at the mid-height of the channel. These results show a qualitative and quantitative good agreement with those

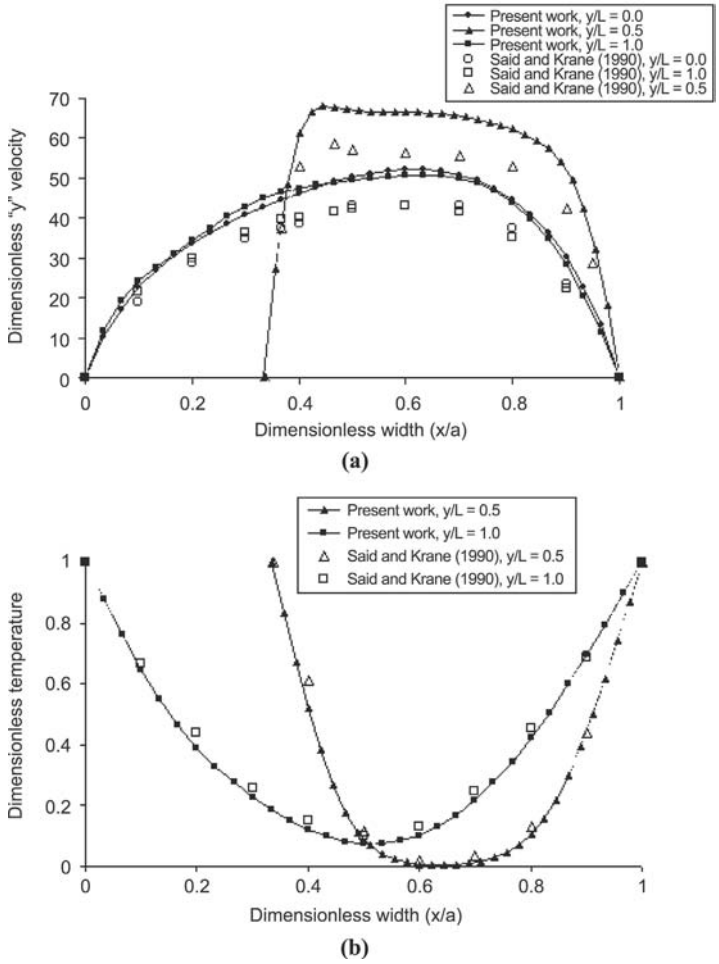

Figure 8.
Natural convection in vertical channels. Channel with a circular obstruction at the middle of its height with an Ar of 0.2727 for $Ra = 2 \times 10^4$: profiles at different sections of (a) vertical velocity component and (b) temperature

previously published. The discrepancies observed in the vertical velocity distribution of Figure 8(a) are attributed to the coarse mesh used in Said and Krane (1990).

The effects of multiple obstructions in vertical channels are studied at $Ra = 10^2$, 10^3, 10^4, 10^5 and 10^6 (case C). Different distributions for the obstructions are considered in this work (see Figure 1 and Table I). The obtained local Nu distributions along vertical walls are plotted in Figures 9, 10, 11 and 12 corresponding to Geometry I, II, III and IV, respectively. For these four situations, the local Nu increases for larger Ra at the upstream region of the obstructions. In general, the presence of obstructions inhibits the heat transfer along the walls due to the stagnant fluid developed near the intersection of

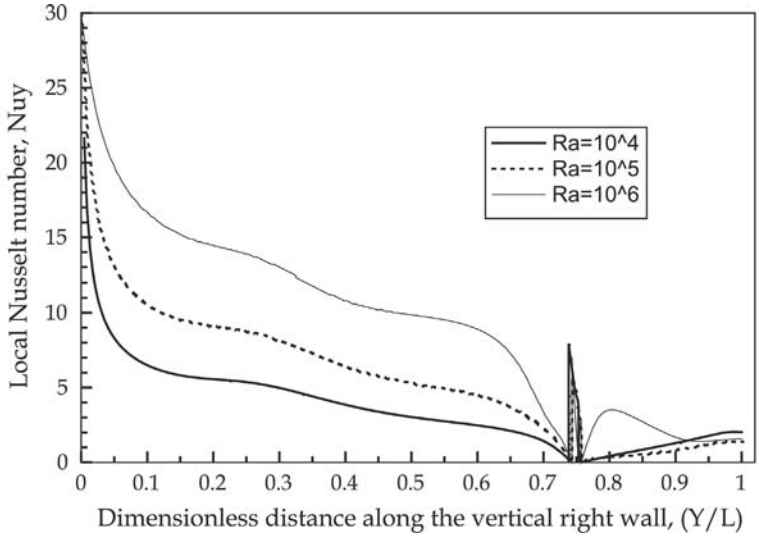

Figure 9.
Natural convection in vertical channels. Local Nu distribution in the Geometry I (Ar = 0.2) of a channel with multiple obstructions

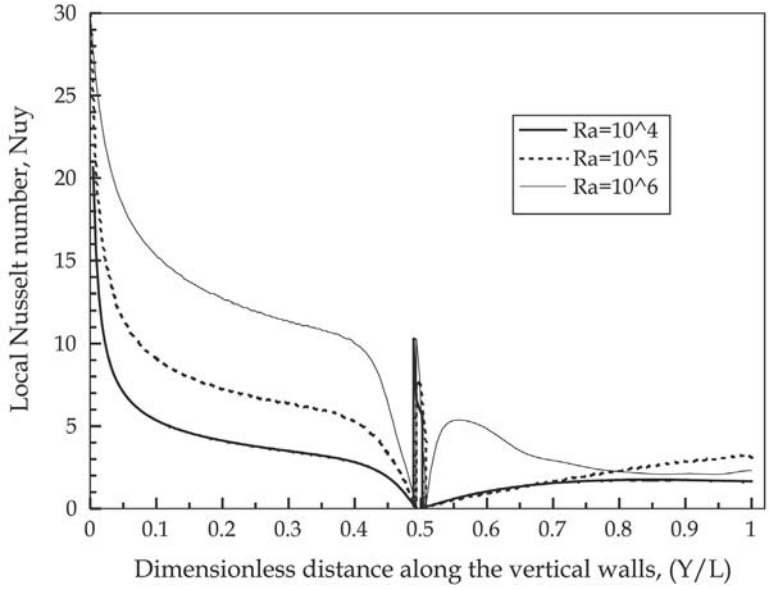

Figure 10.
Natural convection in vertical channels. Local Nu distribution in the Geometry II (Ar = 0.2) of a channel with multiple obstructions

the obstacle with the wall. However, at high Ra the heat transfer is enhanced in the downstream zone of the obstructions due to the vortex formation developed behind them while the increment of the vertical velocity near the tip of the obstruction leads to an increase in the local Nu coefficient. Figures 13 and 14 show the average Nu plotted against the Ra for Ar=0.2 and 0.3, respectively.

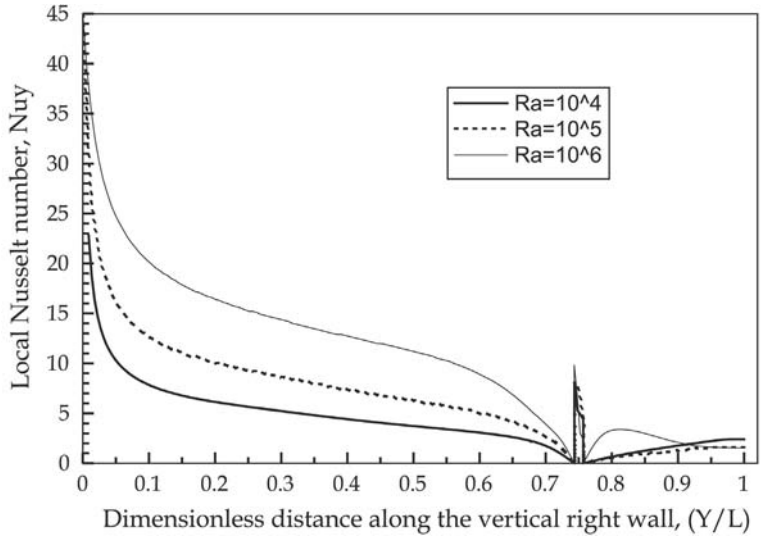

Figure 11.
Natural convection in vertical channels. Local Nu distribution in the Geometry III (Ar = 0.3) of a channel with multiple obstructions

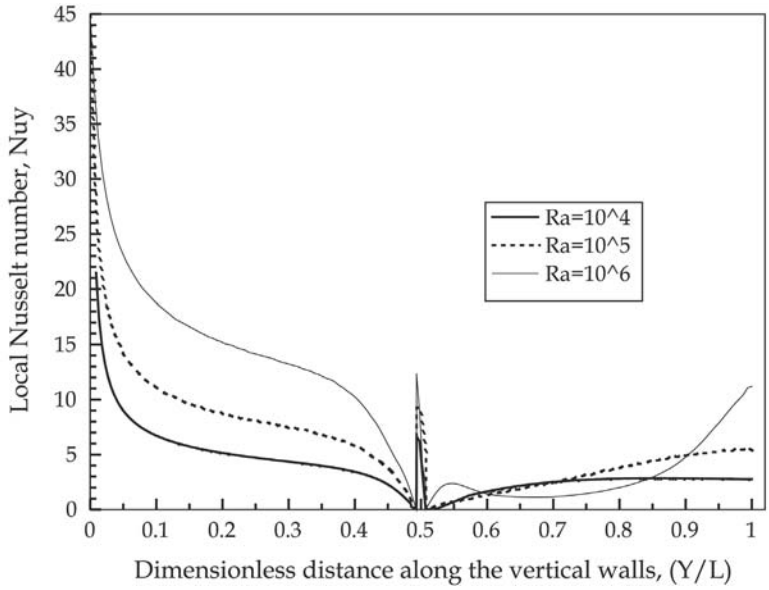

Figure 12.
Natural convection in vertical channels. Local Nu distribution in the Geometry IV (Ar = 0.3) of a channel with multiple obstructions

When the obstructions are located in the middle of the channel height, the average Nu is lower than that obtained for the non-centred positions. This effect is more evident for the case with Ar = 0.2 due to the influence of the obstructions given by their large w/a ratio, i.e. the heat transfer conditions are

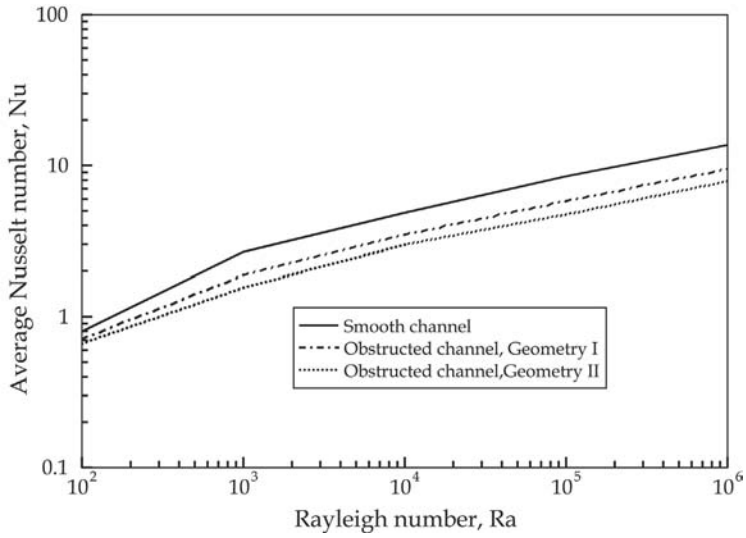

Figure 13.
Natural convection in vertical channels. Average Nu with Ar = 0.2 for different Ra in Geometries I and II

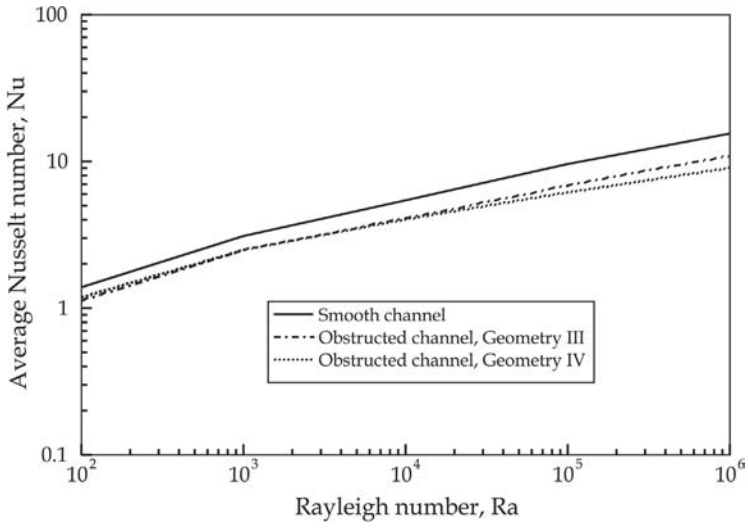

Figure 14.
Natural convection in vertical channels. Average Nu with Ar = 0.3 for different Ra in Geometries III and IV

improved at greater Ar where the effects of the obstruction distributions decrease. Although the heat transfer area is lower in the unobstructed channel when compared to that for the obstructed duct, higher average Nu are obtained for the first case owing to the larger associated mass flow rates. The isotherms (plotted 0.1 apart), streamlines and pressure contours for different Ra are shown in Figures 15, 16, 17 and 18 for Geometries I, II, III and IV, respectively. In these

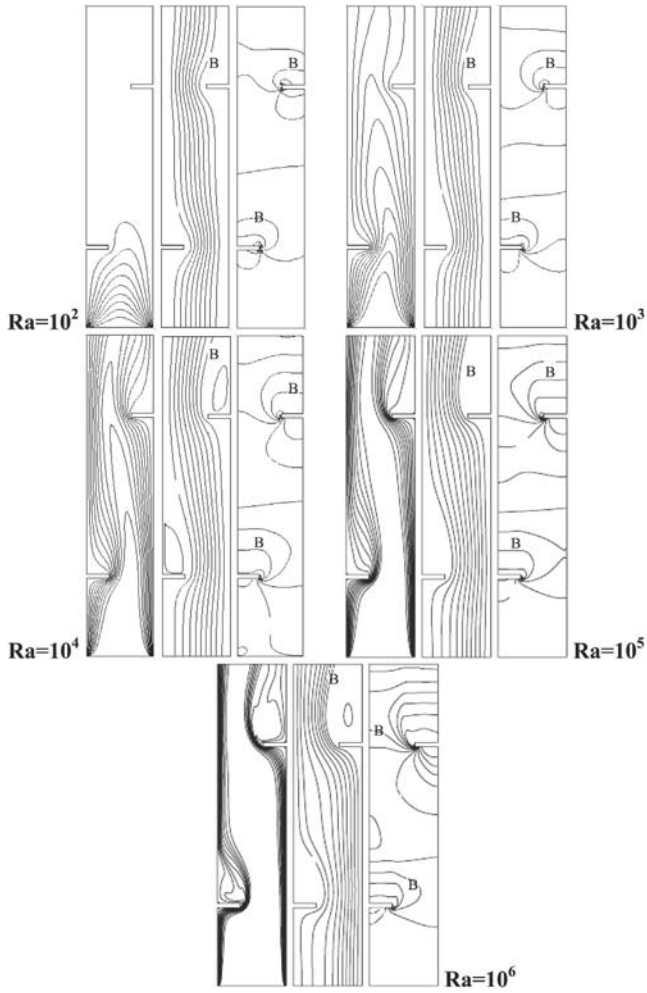

Ra	φ_A	φ_A	$\Delta\varphi$	p_A	p_B	Δp
10^2	-0.018	-0.163	0.018	0.018	-0.149	0.083
10^3	-0.083	-0.872	0.100	0.025	-0.239	0.088
10^4	-0.250	-2.952	0.336	-0.001	-0.214	0.071
10^5	-0.728	-7.960	0.904	0.009	-0.158	0.056
10^6	-1.836	-19.600	2.204	0.019	-0.431	0.031

Figure 15.
Natural convection in vertical channels. Geometry I of a channel with multiple obstructions for different Ra: isotherms (plotted 0.1 apart), streamlines and pressure contours

cases, practically all the heat transfer takes place near the entrance region for low Ra values. As the Ra increases, the heat transfer occurs throughout the channel length and the thermal fields show higher temperature gradients near the walls while the streamlines patterns denote increasing flow re-circulations in the upper zones of the obstructed sections. The pressure contours present

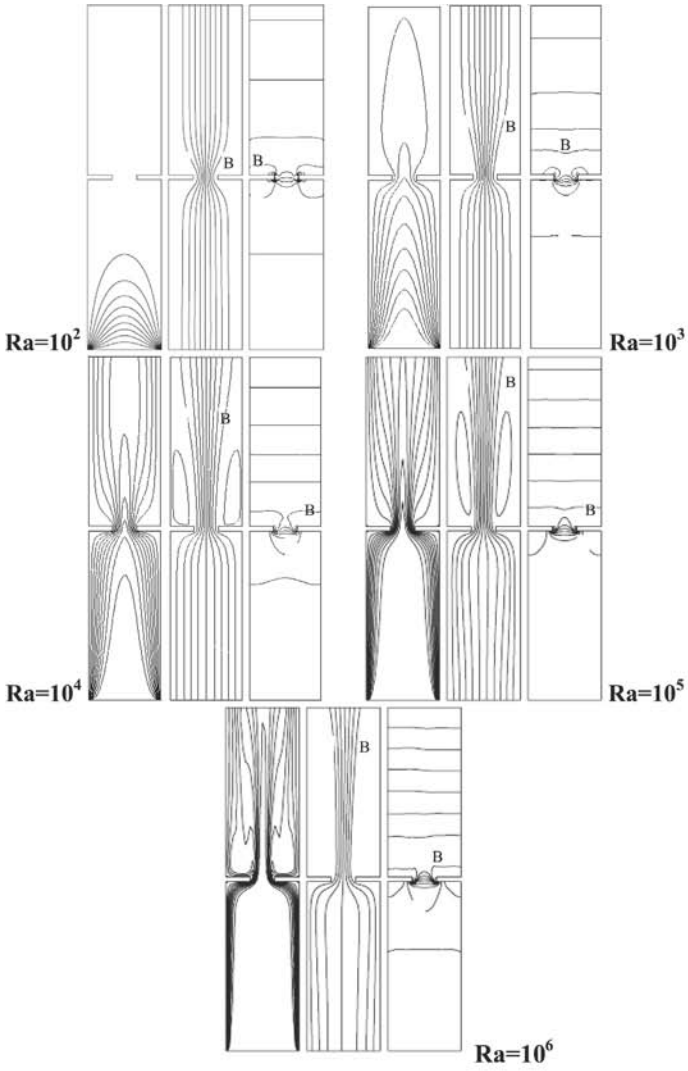

Ra	φ_A	φ_B	$\Delta\varphi$	p_A	p_B	Δp
10^2	-0.011	-0.100	0.011	0.202	-0.374	0.115
10^3	-0.043	-0.592	0.069	0.051	-0.432	0.121
10^4	-0.094	-1.932	0.230	0.036	-0.481	0.102
10^5	-0.240	-5.160	0.616	0.037	-0.347	0.077
10^6	-0.892	-12.760	1.976	0.003	-0.327	0.047

Figure 16.
Natural convection in vertical channels. Geometry II of a channel with multiple obstructions for different Ra: isotherms (plotted 0.1 apart), streamlines and pressure contours

minimum values at the tip of the wall obstructions in agreement with the maximum values of the velocity vectors in the vicinity of such region. These patterns reproduce the effect of transversal area reduction on the flow at obstructed levels. It is important to remark that the numerical results obtained

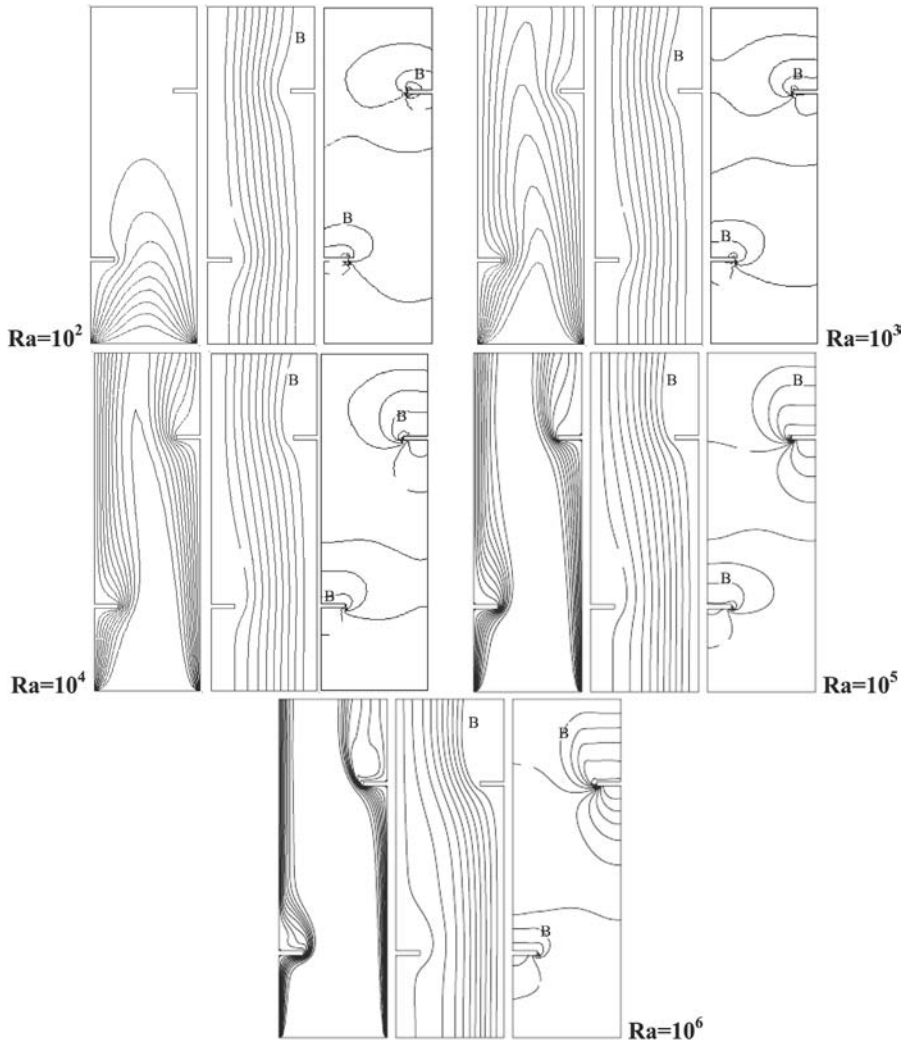

Ra	φ_A	φ_B	$\Delta\varphi$	p_A	p_B	Δp
10^2	-0.043	-0.390	0.043	0.050	-0.167	0.109
10^3	-0.207	-1.935	0.216	0.034	-0.259	0.098
10^4	-0.722	-7.074	0.801	0.035	-0.235	0.090
10^5	-1.782	-19.620	1.980	0.012	-0.098	0.055
10^6	-4.329	-46.890	4.680	0.003	-0.034	0.037

Figure 17.
Natural convection in vertical channels. Geometry III of a channel with multiple obstructions for different Ra: isotherms (plotted 0.1 apart), streamlines and pressure contours

in the present analysis are in good agreement with those reported in Viswatmula and Amin (1995) for Ra = 10^2 to 10^4.

It is worth mentioning that the numerical responses provided by the finite element formulation described in Section 2 do not exhibit a strong mesh

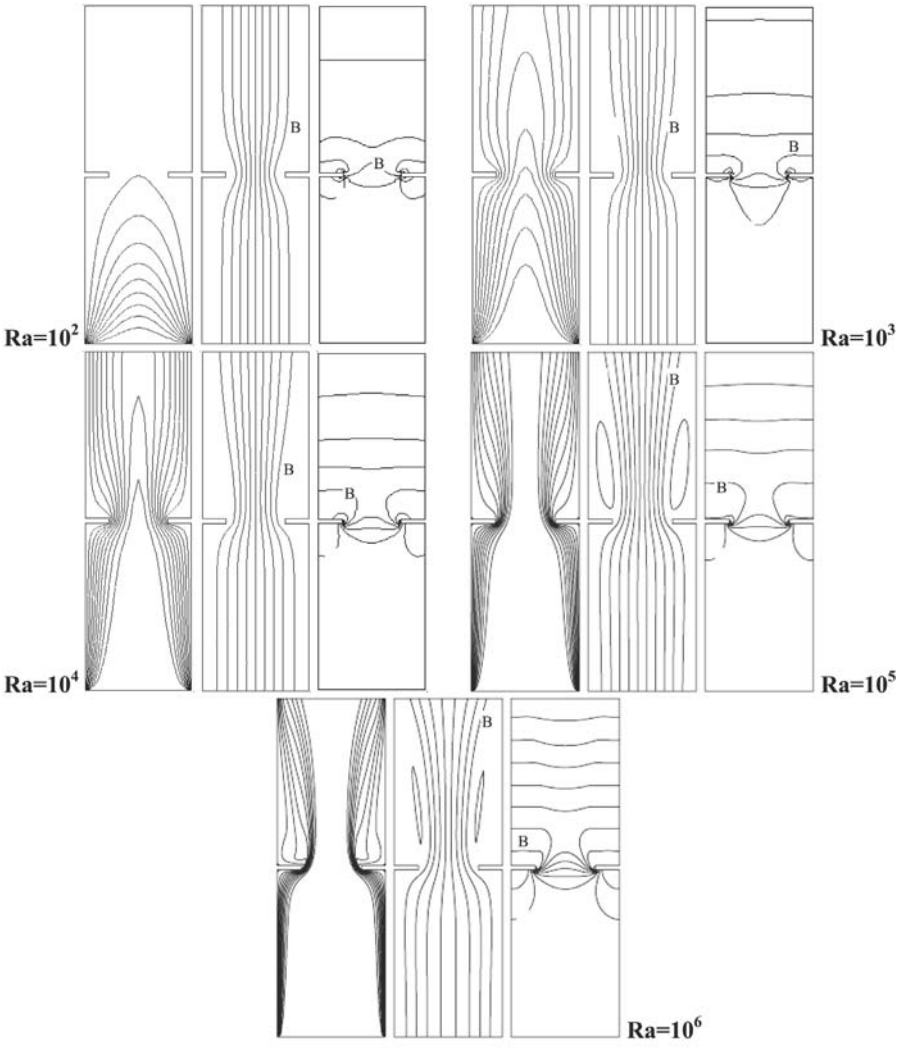

Ra	φ_A	φ_B	$\Delta\varphi$	p_A	p_B	Δp
10^2	-0.038	-0.350	0.039	0.062	-0.211	0.136
10^3	-0.182	-1.755	0.189	-0.019	-0.395	0.126
10^4	-0.538	-5.994	0.684	0.042	-0.374	0.104
10^5	-1.251	-17.550	1.809	0.037	-0.350	0.097
10^6	-4.707	-45.630	5.850	0.018	-0.377	0.056

Figure 18.
Natural convection in vertical channels. Geometry IV of a channel with multiple obstructions for different Ra: isotherms (plotted 0.1 apart), streamlines and pressure contours

dependency. In particular, in case C, small oscillations in the pressure field are only observed in the vicinity of the obstructions for significant reductions (e.g. 50 per cent) in the number of elements in the channel width. Additionally, some numerical features of the simulations for case C (Geometry I) at different Ra

are shown in Table III. Similar convergence trends have been also observed for Geometries II-IV. The computational effort required for $Ra = 10^6$ is presumably attributed to the large vortexes developed behind the obstructions. Figure 19 depicts a typical evolution of the residual norm during the iterative process where a reasonable convergence rate is achieved by the staggered schemed used to solve the thermally-coupled flow formulation.

3.2 Mixed convective flow around a heated squared obstruction in a horizontal channel

Non-isothermal flows past a rectangular cylinder have been extensively analysed in order to evaluate the buoyancy effects on the physical behaviour of internal mixed convection (Chang *et al.*, 1988; Leung *et al.*, 2000; Ramaswamy and Jue, 1992; Shuja *et al.*, 2000). This problem is also studied here to assess the numerical response of the proposed methodology in these kind of flows by performing a comparison with the results reported in Ramaswamy and Jue (1992). The geometry and boundary conditions are sketched in Figure 20 considering a vertical downward gravity action. Traction-free conditions are assumed at the outflow section. The thermal buoyancy is normal to the forced flow direction and, under specific conditions, may distort the main stream in

Table III.
Natural convection in vertical channels. Numerical features of the simulations for case C (Geometry I) at different Ra

Ra				
10^2	10^3	10^4	10^5	10^6
Steady-state 18 iterations	Steady state 37 iterations	Steady-state 40 iterations	Steady-state 46 iterations	Transient 480 steps 6 iterations/step

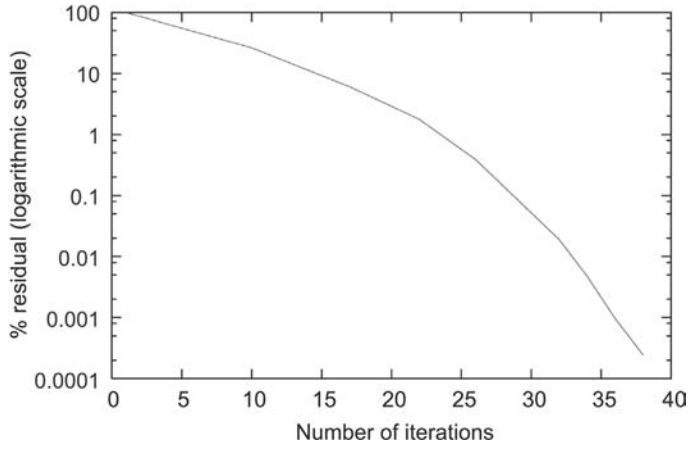

Figure 19.
Natural convection in vertical channels. Evolution of the residual norm (in per cent) for Geometry I with $Ra = 10^4$

the wake of the bluff body. An important consideration in this analysis is related to the limits of the flow conditions for which neither the forced nor the natural convection mechanisms are usually dominant and both need to be taken into account in conjunction. Therefore, the air flow and heat transfer characteristics at different Gr are studied in this problem for Re = 100 and 500 with Pr = 0.71.

The computational domain consists of approximately 7,500 four-noded standard isoparametric regular elements (7,750 nodes) with 40 elements distributed in the channel height.

Local Nu distributions along the lower and upper walls are presented in Figure 21 for Re = 100. As can be seen, these profiles are locally affected by the rectangular cylinder. From the channel inlet, the distribution of the Nu is continuously decreased before confronting the obstacle, according to the trend of a thermally developing channel flow. Before the flow reaches the obstruction, Nu starts increasing and attains a maximum value almost at the end of the cylinder, where it again decays towards its asymptotic value of a fully developed channel flow. The lower and upper curves coincide for Gr = 0. For increasing Gr, they show a gradual asymmetric behaviour owing to the stronger influence of the natural convection, i.e. Nu increases on the lower wall and decreases on the upper one. An overall good agreement with the results obtained in Ramaswamy and Jue (1992) can be observed. Nevertheless, some discrepancies appear in regions close to the obstacle which can be explained by the different physically consistent expressions used in the present analysis to compute the bulk temperature along the channel (see Nomenclature section).

Figure 22 shows friction coefficient distributions along the lower and upper walls for Re = 100. Once more, symmetric profiles are obtained for Gr = 0. The friction coefficients along the lower wall grow with increasing Gr while the reverse trend is observed along the upper wall. These effects are due to the increment of the mass flow rate in the channel section below the rectangular cylinder when the natural convection becomes relevant. Furthermore, the friction coefficient along the upper wall reaches negative values when a re-circulating flow appears in the upstream upper channel zone for $Gr > 8 \times 10^4$

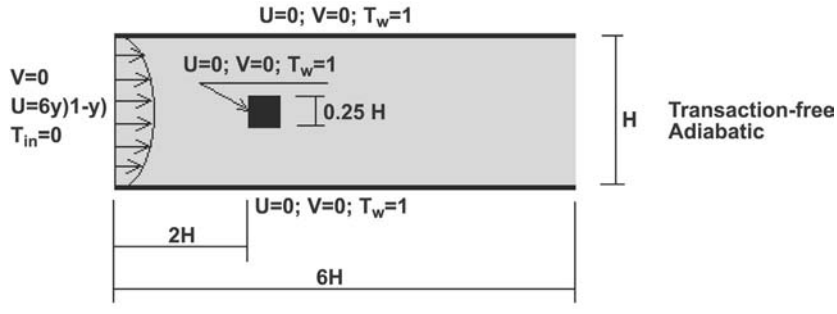

Figure 20.
Mixed convective flow around a heated squared obstruction in a horizontal channel. Geometry and boundary conditions

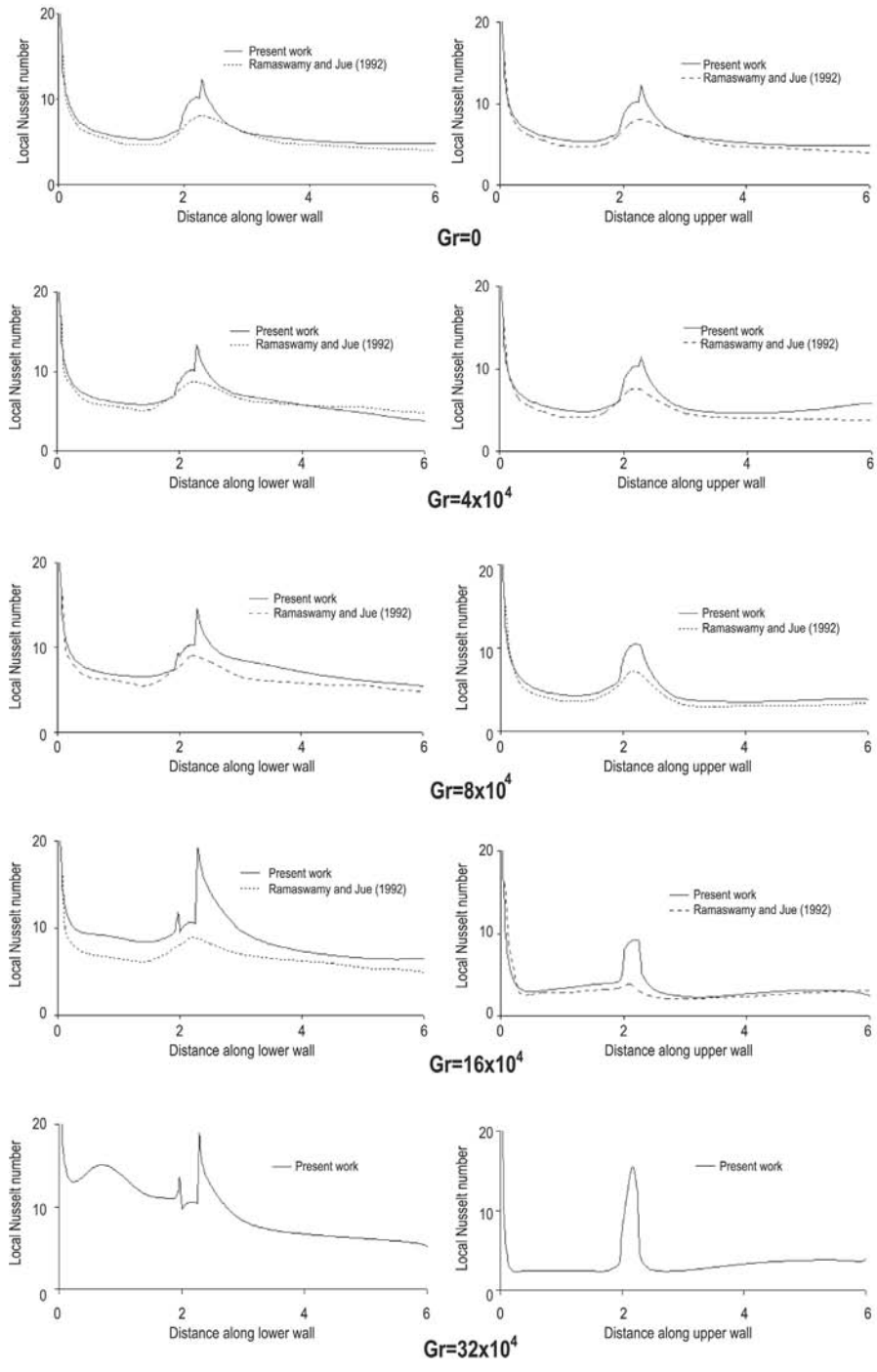

Figure 21.
Mixed convective flow around a heated squared obstruction in a horizontal channel. Local Nu for Re = 100 at different Gr

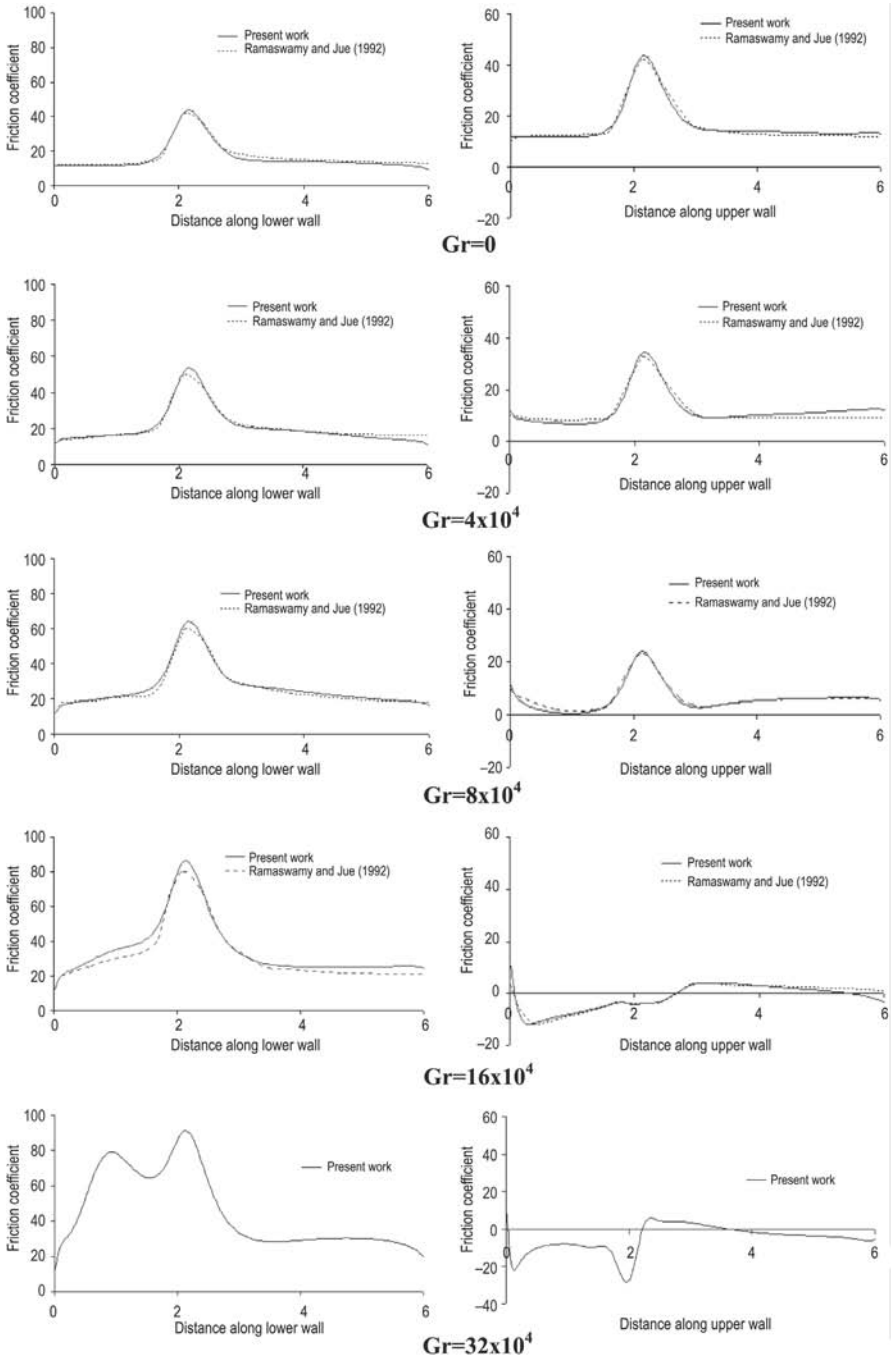

Figure 22.
Mixed convective flow around a heated squared obstruction in a horizontal channel. Friction coefficients for Re = 100 at different Gr

approximately. This vortex formation occurs from the inlet region and becomes small near the cylinder because of the transversal area constriction. Then, the flow re-attaches in the downstream zone. The present predictions satisfactorily adjust the available results reported in Ramaswamy and Jue (1992) for Gr ranging from 0 to 16×10^4.

The isotherms (plotted 0.1 apart), streamlines and pressure contours are presented in Figure 23 for $\mathrm{Re} = 100$ at different Gr. The temperature distributions are strongly affected by the buoyancy effects, making evident the local Nu behaviour shown in Figure 21, as the temperature gradient decreases near the upper wall and increases close to the lower wall for higher Gr. The influence of the buoyancy forces on the flow pattern is also reflected in the streamline contours which show increasing mass flow rates below the obstruction for larger Gr. As commented above, this effect is apparent in the friction coefficient distributions described in Figure 22. The pressure contours lose the symmetry obtained for the purely forced convection case ($\mathrm{Gr} = 0$) when Gr increases. All these temperature and flow patterns are qualitatively in agreement with those obtained in Ramaswamy and Jue (1992).

The influence of natural convection is additionally assessed for $\mathrm{Re} = 500$. The corresponding local Nu and friction coefficient distributions along both channel walls are, respectively, shown in Figures 24 and 25. The symmetry found in such curves demonstrates that the buoyancy effects do not play an important role in the flow and heat patterns even for the largest Gr considered.

The drag and lift coefficients for different Gr and Re are summarized in Table IV. As expected, no lift forces are found for $\mathrm{Gr} = 0$. As Gr increases, for $\mathrm{Re} = 100$, the lift coefficient grows accordingly due to the relevancy of the buoyancy forces. This trend is not found for $\mathrm{Re} = 500$ where C_l is almost negligible denoting the major influence of the forced convection in this case which also justifies the practically invariant behaviour of C_d. The drag coefficient for $\mathrm{Re} = 100$ shows an increasing response for higher Gr. Nevertheless, for $\mathrm{Gr} = 32 \times 10^4$, C_d diminishes owing to pressure homogenisation around the obstruction.

All the results presented for this problem are stable steady-state solutions, i.e. no regular periodic shedding has been observed for the range of Gr and Re studied. This can be explained by the proximity of the channel walls with respect to the obstruction height.

4. Conclusions

The numerical simulation of two-dimensional steady-state natural and mixed convection in obstructed channels has been presented by using a finite element thermally coupled incompressible flow formulation obtained via a generalized streamline operator technique.

Natural convection has been studied in several vertical channel configurations for a wide range of Ra. The presence of obstructions in the

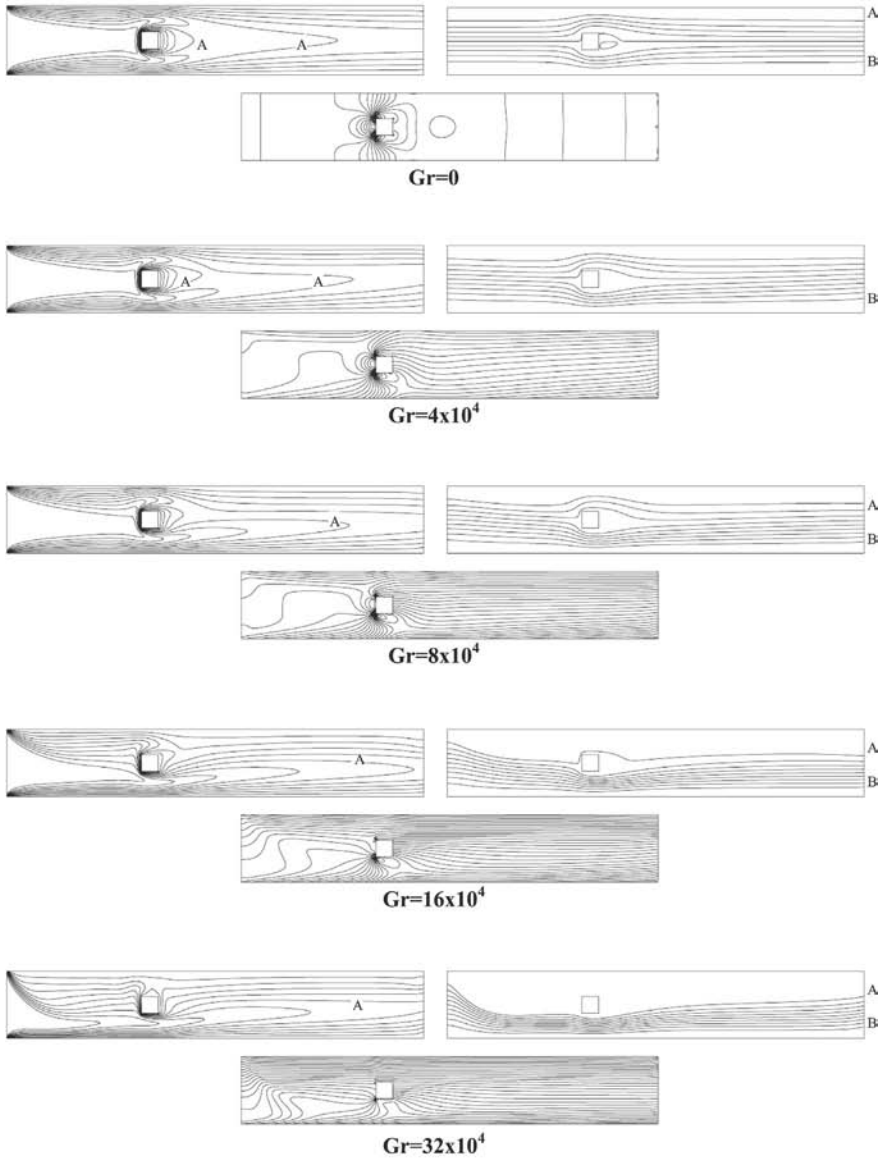

Gr	0	$4x10^4$	$8x10^4$	$16x10^4$	$32x10^4$
p_{max}	2.64	3.84	5.53	10.80	20.20
p_{min}	-1.73	-1.36	-1.06	-1.04	-1.62

Figure 23.
Mixed convective flow around a heated squared obstruction in a horizontal channel. Isotherms ($T_A = 0.5$, plotted $\Delta T = 0.1$ apart), streamlines ($\varphi_A = 0.9$, $\varphi_B = 0.1$, plotted $\Delta\varphi = 0.1$ apart) and pressure contours (30 lines plotted with the minimum value being situated at the left bottom corner of the obstruction) for Re=100 at different Gr

channel causes better local heat transfer rates due to increments in both the vertical flow and surface area on the obstructed wall. However, the average Nu decreases when compared to that for the unobstructed channel owing to the reduction of mass flow rate and the existence of stagnant regions caused by the obstructions.

Mixed convection has been analysed in a horizontal channel with a built-in rectangular cylinder for different Re and Gr. The proposed methodology has been validated in the analysis of mixed convection problems involving low and high Gr/Re^2 relations which, respectively, denote the relevance of either natural or forced convection.

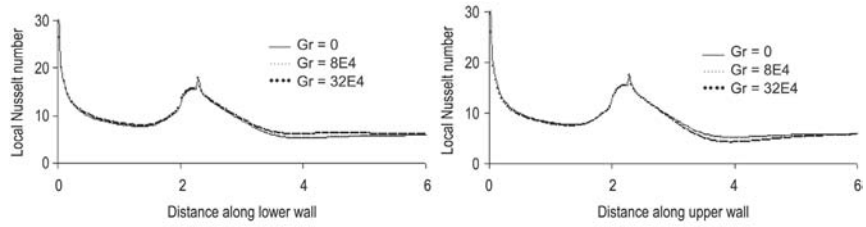

Figure 24.
Mixed convective flow around a heated squared obstruction in a horizontal channel. Local Nu for Re = 500 at different Gr

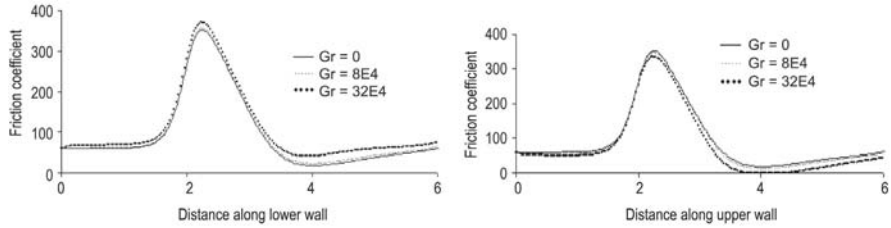

Figure 25.
Mixed convective flow around a heated squared obstruction in a horizontal channel. Friction coefficients for Re = 500 at different Gr

Table IV.
Mixed convective flow around a heated squared obstruction in a horizontal channel. Drag and lift coefficients for different Re and Gr

Re	Gr	C_d	C_l
100	0	1.2303	0
	4×10^4	1.2451	0.5415
	8×10^4	1.2916	1.0074
	16×10^4	1.4278	2.0508
	32×10^4	1.0392	2.7593
500	0	0.9789	0
	8×10^4	0.9793	0.0205
	32×10^4	0.9836	0.0803

The results obtained in this work for both problems have been successfully validated with available experiments and other existing numerical solutions. The performance of the methodology applied in the simulations has been also illustrated in terms of grid independency, computational effort and convergence rates. Nevertheless, the transient behaviour at Ra higher than those considered in this work as well as the study of the influence of the channel height on the thermal and flow patterns need to be explored in further research.

References

Aung, W. and Worku, G. (1986), "Developing flow and flow reversal in a vertical channel with asymmetric wall temperatures", *ASME Journal of Heat Transfer*, Vol. 108, pp. 299-304.

Baek, B., Armaly, B. and Chen, T. (1993), "Measurements in buoyancy-assisting separated flow behind a vertical backward-facing step", *ASME Journal of Heat Transfer*, Vol. 115, pp. 403-8.

Behr, M., Franca, L.P. and Tezduyar, T. (1993), "Stabilized finite element methods for the velocity-pressure-stress formulation of incompressible flows", *Computer Methods in Applied Mechanics and Engineering*, Vol. 104, pp. 31-48.

Bejan, A., Fowler, A. and Stanescu, G. (1995), "The optimal spacing between horizontal cylinders in a fixed volume cooled by natural convection", *International Journal of Heat and Mass Transfer*, Vol. 38 No. 11, pp. 2047-55.

Brooks, A.N. and Hughes, T.J.R. (1982), "Streamline upwind/Petrov-Galerkin formulations for convection dominated flows with particular emphasis on the incompressible Navier-Stokes equations", *Computer Methods in Applied Mechanics and Engineering*, Vol. 32, pp. 199-259.

Burch, T., Rhodes, T. and Acharya, S. (1985), "Laminar natural convection between finitely conducting vertical plates", *International Journal of Heat and Mass Transfer*, Vol. 28 No. 6, pp. 1173-86.

Celentano, D., Cruchaga, M., Moraga, N. and Fuentes, J. (2001), "Modeling natural convection with solidification in mould cavities", *Numerical Heat Transfer*, Part A, Vol. 39, pp. 631-54.

Cesini, G., Paroncini, M., Cortella, G. and Manzan, M. (1999), "Natural convection from a horizontal cylinder in a rectangular cavity", *International Journal of Heat and Mass Transfer*, Vol. 42, pp. 1801-11.

Chang, K., Choi, C. and Cho, C. (1988), "Laminar natural convection heat transfer from sharp-edged horizontal bars with flow separation", *International Journal of Heat and Mass Transfer*, Vol. 31 No. 6, pp. 1177-87.

Cruchaga, M. (1998), "A study of the backward-facing step problem using a generalized streamline formulation", *Communications in Numerical Methods in Engineering*, Vol. 14 No. 8, pp. 697-708.

Cruchaga, M. and Celentano, D. (2000), "A finite element thermally coupled flow formulation for phase-change problems", *International Journal for Numerical Methods in Fluids*, Vol. 34, pp. 279-305.

Cruchaga, M. and Oñate, E. (1997), "A finite element formulation for incompressible flow problems using a generalized streamline operator", *Computer Methods in Applied Mechanics and Engineering*, Vol. 143, pp. 49-67.

Cruchaga, M. and Oñate, E. (1999), "A generalized streamline finite element approach for the analysis of incompressible flow problems including moving surfaces", *Computer Methods in Applied Mechanics and Engineering*, Vol. 173, pp. 241-55.

Elenbass, W. (1942), "Heat dissipation of parallel plates by free convection", *Physica*, Vol. 9, pp. 1-28.

Hong, B., Armaly, B. and Chen, T. (1993), "Laminar mixed convection in a duct with a backward-facing step: the effects of inclination angle and Prandtl number", *International Journal of Heat and Mass Transfer*, Vol. 36 No. 12, pp. 3059-67.

Huang, H. and Usmani, A. (1994), *Finite Element Analysis for Heat Transfer: Theory and Software*, Springer-Verlag, London.

Hughes, T.J.R. and Mallet, M. (1986), "A new finite element formulation for computational fluid dynamics: V. Circumventing the BB condition: a stable Petrov-Galerkin formulation of the Stokes problem accommodating equal-order interpolation", *Computer Methods in Applied Mechanics and Engineering*, Vol. 59, pp. 85-99.

Islam, M., Monde, M., Hasan, M. and Mitsutake, Y. (1998), "Experimental study of critical heat flux in convective-tube open thermosyphon", *International Journal of Heat and Mass Transfer*, Vol. 41, pp. 3691-704.

Iwai, H., Nakabe, K. and Suzuki, K. (2000a), "Flow and heat transfer characteristics of backward-facing step laminar flow in a rectangular duct", *International Journal of Heat and Mass Transfer*, Vol. 43, pp. 457-71.

Iwai, H., Nakabe, K., Suzuki, K. and Matsubara, K. (2000b), "The effects of duct inclination angle on laminar mixed convective flows over a backward-facing step", *International Journal of Heat and Mass Transfer*, Vol. 43, pp. 473-85.

Kaminski, D., Fu, X. and Jensen, M. (1995), "Numerical and experimental analysis of combined convective and radiative heat transfer in laminar flow over a circular cylinder", *International Journal of Heat and Mass Transfer*, Vol. 38 No. 17, pp. 3161-9.

Karniadakis, G. (1988), "Numerical simulation of forced convection heat transfer from a cylinder in crossflow", *International Journal of Heat and Mass Transfer*, Vol. 31 No. 1, pp. 107-18.

Leung, C., Chen, S. and Chan, T. (2000), "Numerical simulation of laminar forced convection in a air-cooled horizontal printed circuit board assembly", *Numerical Heat Transfer*, *Part A*, Vol. 37, pp. 373-93.

Malvern, L. (1969), *Introduction to the Mechanics of a Continuous Medium*, Prentice-Hall, Englewood Cliffs.

Maughan, J. and Incropera, F. (1987), "Experiments on mixed convection heat transfer for airflow in a horizontal and inclined channel", *International Journal of Heat and Mass Transfer*, Vol. 30 No. 7, pp. 1307-18.

Mohamad, A. and Sezai, I. (1997), "Natural convection in C-shaped thermosyphon", *Numerical Heat Transfer*, *Part A*, Vol. 32, pp. 311-23.

Naylor, D. and Tarasuk, J. (1993a), "Natural convective heat transfer in a divided vertical channel: part I – numerical study", *ASME Journal of Heat Transfer*, Vol. 115, pp. 377-87.

Naylor, D. and Tarasuk, J. (1993b), "Natural convective heat transfer in a divided vertical channel: part II – experimental study", *ASME Journal of Heat Transfer*, Vol. 115, pp. 388-94.

Ramaswamy, B. and Jue, T.C. (1992), "Some recent trends and developments in finite element analysis for incompressible thermal flows", *International Journal for Numerical Methods in Engineering*, Vol. 35, pp. 671-707.

Sadeghipour, M. and Hannani, S. (1992), "Transient natural convection from a horizontal cylinder confined between vertical walls – a finite element solution", *International Journal for Numerical Methods in Engineering*, Vol. 34, pp. 621-35.

Said, S.A.M. and Krane, R.J. (1990), "An analytical and experimental investigation of natural convection heat transfer in vertical channels with a single obstruction", *International Journal of Heat and Mass Transfer*, Vol. 33 No. 6, pp. 1121-34.

Shuja, S., Yilbas, B. and Iqbal, M. (2000), "Heat transfer characteristics of flow past a rectangular protruding body", *Numerical Heat Transfer*, *Part A*, Vol. 37, pp. 307-21.

Tezduyar, T., Mittal, S., Ray, S.E. and Shih, R. (1992), "Incompressible flow computations with stabilized bilinear and linear equal-order interpolation velocity-pressure elements", *Computer Methods in Applied Mechanics and Engineering*, Vol. 95, pp. 221-42.

Tsui, Y. and Wang, C. (1995), "Calculation of laminar separated flow in symmetric two-dimensional diffusers", *ASME Journal of Fluids Engineering*, Vol. 117, pp. 612-16.

Viswatmula, P. and Amin, M.R. (1995), "Effects of multiple obstructions on natural convection heat transfer in vertical channels", *International Journal of Heat and Mass Transfer*, Vol. 38 No. 11, pp. 2039-46.

Wang, B. and Liu, T. (1992), "Research on hydrodynamics and heat transfer for fluid flow around heating spheres in tandem", *International Journal of Heat and Mass Transfer*, Vol. 35 No. 2, pp. 307-17.

Zienkiewicz, O. and Taylor, R. (1989), *The Finite Element Method*, 4th ed., McGraw-Hill, London, Vol. 1 and 2.